Streaming from the Equator of a Drop in an External Electric Field

Quentin Brosseau and Petia M. Vlahovska

Phys. Rev. Lett. **119**, 034501 — Published 20 July 2017

DOI: 10.1103/PhysRevLett.119.034501

Streaming from the equator of a drop in an external electric field

Quentin Brosseau and Petia M. Vlahovska*
*School of Engineering, Brown University, RI 02912, USA**
(Dated: June 20, 2017)

Tip streaming generates micron- and submicron- sized droplets when a thin thread pulled from the pointy end of a drop disintegrates. Here, we report streaming from the equator of a drop placed in a uniform electric field. The instability generates concentric fluid rings encircling the drop, which break up to form an array of microdroplets in the equatorial plane. We show that the streaming results from an interfacial instability at the stagnation line of the electrohydrodynamic flow, which creates a sharp edge. The flow draws from the equator a thin sheet which destabilizes and sheds fluid cylinders. This streaming phenomenon provides a new route for generating monodisperse microemulsions.

A drop in a uniform electric field can form conical tips at the poles (Taylor cones) emitting jets of charged tiny droplets [1–4]. This so called electrohydrodynamic (EHD) tip streaming or cone-jetting occurs in many natural phenomena (e.g., drops in thunderclouds) and technological applications (printing, electrospraying, electrospinning) [1, 5].

The streaming is related to a generic interfacial instability due to a convergent flow [6], see Figure 1.a. The interface is compressed and a local perturbation at the stagnation point (e.g., drop tips) gets drawn by the flow. When the viscous stresses overcome the interfacial tension, the perturbation grows into a fluid filament. This is the tip streaming phenomenon commonly observed in the microfluidic co-flow geometry [7–9]. If instead of a point, the flow is converging to a stagnation line, then a thin sheet can be entrained [10]. By analogy with the cone-jet geometry resulting from the destabilization of a stagnation point, it is expected that the instability of a stagnation line would give rise to an edge-sheet structure. In this Letter, we report streaming resulting from a stagnation line instability at the equator of a drop: EHD equatorial streaming, which creates "Saturn-rings" around the drop (see Figure 1.b).

Experimentally, we exploit the electrohydrodynamic flow about a neutral drop placed in a uniform electric field [11, 12]. By varying the fluid conductivities, we are able to create a flow converging either at the drop poles (Figure 1.c) to generate cone-jet, or at the equator (Figure 1.d) to generate an edge-sheet. The latter case is the focus of this work.

The electrohydrodynamic flow is driven by electric shear stresses due to induced surface charges[11, 12]. For a drop in a uniform electric field the resulting flow is axisymmetrically aligned with the applied field. For a spherical drop with radius a placed in DC electric field $\mathbf{E} = E\hat{\mathbf{z}}$, the surface velocity is [11]

$$\mathbf{u}_T = \frac{a\varepsilon_{\rm ex}E^2}{\mu_{\rm ex}} \frac{9(S-R)}{10(1+\lambda)(R+2)^2} \sin(2\theta)\hat{\boldsymbol{\theta}}, \qquad (1)$$

where $\lambda = \mu_{\rm in}/\mu_{\rm ex}$ is the viscosity ratio between the drop and suspending fluids and θ is the angle with the applied field direction. The direction of the surface flow depends on the difference of conductivity, σ, and permittivity, ε, of the drop and suspending fluids $R = \sigma_{\rm in}/\sigma_{\rm ex}$ and $S = \varepsilon_{\rm in}/\varepsilon_{\rm ex}$. For drops with $R/S > 1$, the surface flow is from the equator to the poles. Accordingly, the poles become stagnation points where streaming occurs at sufficiently strong fields, see Figure 1.c. Since the tips are also the location of maximum induced charge ($Q \sim \cos\theta$), the emitted drops carry away some of it and become charged.

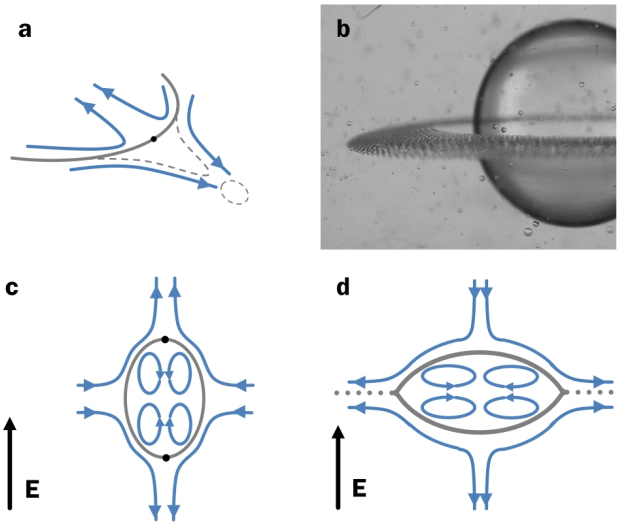

FIG. 1: (Color online) (a) A protrusion at the stagnation point of a convergent flow can grow into a filament. (b) Rings of droplets formed via EHD streaming from the equator of a drop after application of a DC electric pulse. (c) For EHD flow about a drop with $R/S > 1$ the poles are stagnation points where cone-jets form. (d) For EHD flow about a drop with $R/S < 1$ the equator is a stagnation line where edge-sheet is expected to form.

If the drop is less conducting than the suspending medium, $R/S < 1$, the surface flow is from the pole to the equator. Here the equator is a stagnation line. *Could streaming occur in such geometry? What structures are formed?* Surprisingly, drop stability under such conditions has been studied only to a very limited extent. Numerical studies [13–15] show that the drop either dimples at the poles to become a torus, or it flattens into a

pancake shape. An experimental study also mentions a lens-like deformation [16]. Tiny drops are observed near the sharp edge, which hints at the possibility of a streaming instability. Intriguingly, flow convergence in a more complex geometry - flattened droplet formed at the tip of a pendant drop and stretched by an electric field - can lead to rim ejection [17]. However this instability is driven by charge concentration at an equatorial line and the conductivity ratio is $R/S > 1$. Here we show that streaming can occur even for $R/S < 1$ and in the absence of charge at the stagnation line. In this case, EHD equatorial streaming is characterized by the shedding of charge-free rings, which undergo capillary instability and break up into droplets.

Experiment: The fluid system and experimental set up are similar to [18]. Silicone oil (SO) and castor oil (CO) are used as drop and suspending fluids, respectively. Both fluids have low conductivity (in the order of $10^{-12}\,S/m$) and high viscosity (100 to 1000 times that of water) (see [19] for detailed information). CO viscosity is $\mu_{\rm ex} = 0.69\,Pa.s$ and SO viscosity is varied to adjust the viscosity ratio $\lambda = \mu_{\rm in}/\mu_{\rm ex}$ in the range between 0.001 to 10. For this system, the permittivity ratio is $S = \varepsilon_{\rm in}/\varepsilon_{\rm ex} = 0.6$ and the conductivity ratio $R = \sigma_{\rm in}/\sigma_{\rm ex} < S$. R is further lowered by doping the CO with organic electrolyte TBAB (Tetrabuthylamonium Bromide) or AOT (Dioctyl sulfoccinate sodium salt). The surface tension γ in all cases is measured to be 4.5 mN/m confirming that the TBAB and AOT are not surface-active in the SO/CO system. CO was changed for each experiment and the chamber thoroughly cleaned to avoid cross-contamination. A uniform DC electric field is generated in a rectangular chamber built around two parallel ITO coated glass electrodes, both 75x50 mm and set 25mm apart. In the experiment, a millimeter-sized drop is pipetted manually in the middle of the chamber, far away from any boundary. Drop dynamics is recorded by CCD cameras placed either perpendicular to electric field, or parallel to it . On the time scale of the experiment, drop sedimentation is negligible. Figure 2 illustrates the phenomenon of equatorial streaming.

Results: The classic leaky-dielectric theory [11, 12] predicts that in weak electric fields, i.e., electric capillary number $Ca = \varepsilon_{\rm ex}E^2a/\gamma \ll 1$, a drop with $R/S < 1$ adopts an oblate spheroidal shape, the flow and shape being axisymmetrically aligned with the applied field. As the field strength increases, the drop undergoes various types of instabilities depending on fluids viscosities and conductivities. Figure 3.a maps the modes of droplet destabilization as a function of fluids properties. There are three distinct modes:

(A) *Electrorotation* ($R < S$, $Ca > Ca_Q$, any viscosity ratio λ): In this regime, the drop tilts relative to the applied field direction, see Figure 3.b. This symmetry-breaking is due to the Quincke electrorotation [18, 24, 25, 27], which gives rise to a rotational flow about

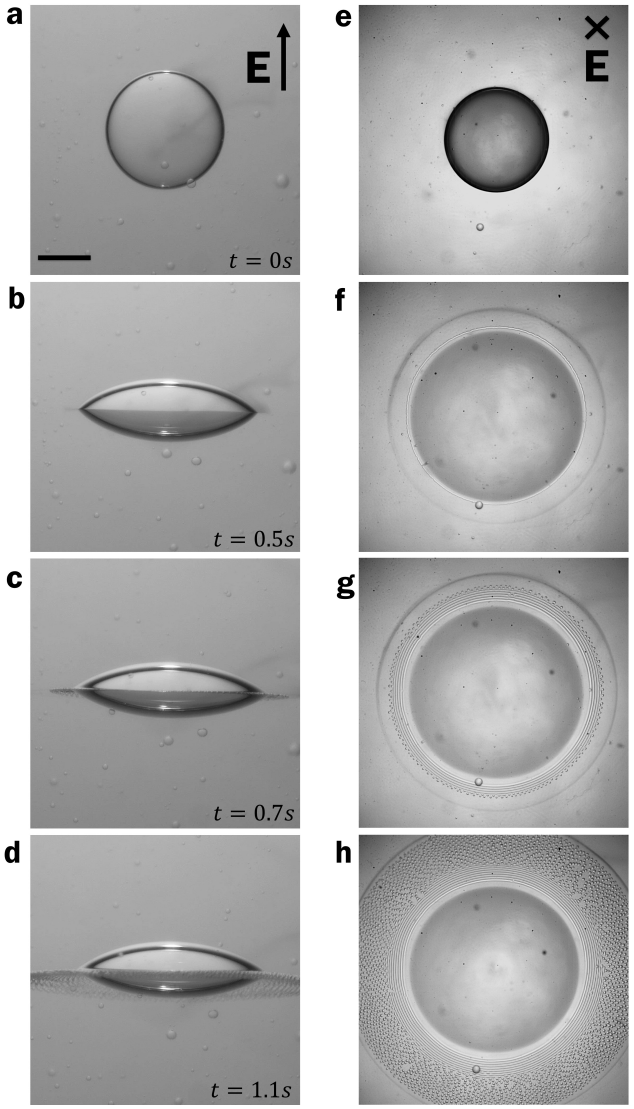

FIG. 2: EHD equatorial streaming observed from direction perpendicular (a-d) and along (e-h) the applied electric field; the field direction is the axis of symmetry. Spherical drops (a,e) deform as the electric field is turned on at $t = 0$. The mother drop flattens to aspect ratio of about 0.5 and forms a lens with a sharp edge (b)-(f). The emission of rings occurs radially in the equatorial plane of the drop (g)-(h). Viscosity ratio is $\lambda = 0.07$. $E = 7.9$ kV/cm, $Ca \sim 4$. Scale bar is 500 μm.

the drop. The Quincke effect stabilizes the drop against break-up and even decreases interface deformation [26]. The threshold for electrorotation, E_Q is estimated from the value for a rigid sphere [28]

$$E_Q^2 = \frac{2\sigma_{\rm ex}\mu_{\rm ex}\left(R+2\right)^2}{3\varepsilon_{\rm ex}^2(S-R)}\,. \qquad (2)$$

For the pure fluid system $E_Q = 3\,kV/cm$ and for a typical drop with radius $a = 1$ mm, $Ca_Q = 0.8$. Adding electrolytes to the suspending fluid increases its conductivity, $\sigma_{\rm ex}$, by several orders of magnitude and shifts the

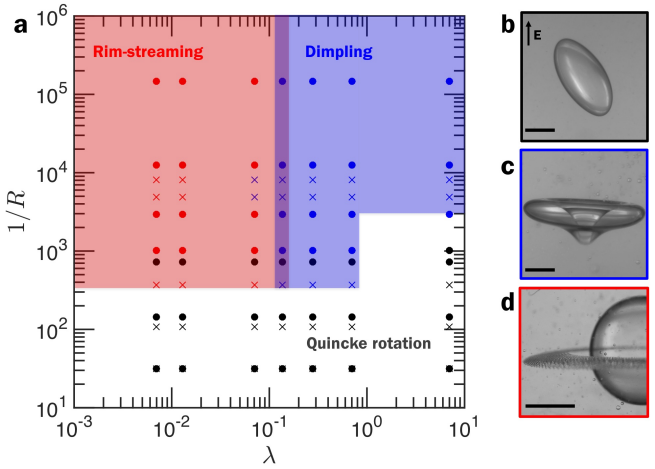

FIG. 3: (Color online) Phase diagram of the drop dynamics in a strong uniformDC electric field: Quincke electrorotation (black), dimpling (blue) for $\lambda > 0.1$, EHD equatorial streaming (red) for $\lambda < 0.1$. The conductivity of the suspending oil is modified by addition of electrolytes TBAB (dots) or AOT (crosses). $E \geq 3$ kV/cm. Scale bar 500 μm. Images (b)-(d) illustrate the drop behaviors.

transition to Quincke to higher field strengths thereby effectively suppressing the electrorotation. The critical conductivity ratio to suppress the electrorotation, R_c, is found from Eq.(2), by solving for R_c with $E = E_c$ being the desired Quincke threshold (e.g, for 1MV/m $R_c = 0.002$). Adding the dopant (TBAB or AOT) decreases the R below the critical value.

In the absence of electrorotation, $R < R_c$ the following two modes of drop fragmentation emerge.

(B) *Dimpling* ($R \ll 1$, $Ca \sim O(1)$, $\lambda \geq 0.1$): In this mode, the drop deforms into a biconcave disc with rounded rim and pinches in its center to form a torus, see Figure 3.c; the torus subsequently breaks into few drops [14, 16, 29]. The drop burst is abrupt, uncontrollable, and the resulting daughter-droplet size and number is irreproducible. This mode creates few drops with size comparable to the mother drop. The critical capillary number is $Ca \sim O(1)$, corresponding to distorting electric stresses that can no longer be contained by the interfacial tension. The observed range of viscosity ratios, above $\lambda \sim O(1)$, for the dimpling is in agreement with numerical simulations [13, 15].

(C) *Equatorial streaming* ($R \ll 1$, $Ca \geq 4$, $\lambda \leq 0.1$): In this mode the drop flattens and forms a sharp edge with thin film attached to it (edge-sheet), see Figure 2. The sheet emits concentric thin rings which break-up into microdroplets, see Figure 4. The ring shedding occurs in a steady manner so droplet production can proceed for tens of seconds. Unlike dimpling, the streaming is a controllable process that is easily triggered and interrupted, e.g., see Figure 1.b which illustrates a mother drop surrounded by daughter droplets after the field is turned off. This streaming mode is able to produce thousands of microdroplets with relatively uniform size distribution, see Figure 5.a. The streaming morphology (sizes of rings and microdroplets, frequency of ring shedding) are insensitive to Ca and R in the explored range of parameters.

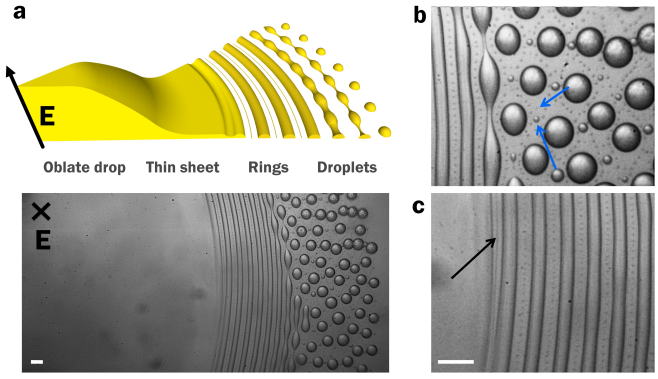

FIG. 4: (Color online)EHD equatorial streaming (a) 3D rendering of the phenomenon as deduced from the experiment [19] ($\lambda = 0.07$). The thin sheet is visible as a slightly brighter region just prior the edge where the ring is forming. A closer inspection reveals (b) two generations of satellite drops created after the ring break-up (blue arrows) and (c) a satellite ring that breaks up in droplets (black arrow). Scale bars 100μm.

Mechanism of the EHD equatorial streaming: The flow velocity at the onset of streaming is about 1 mm/s, which corresponds to Reynolds number $\rho_{\rm ex} U a/\mu_{\rm ex} \sim 10^{-3}$. Hence, the EHD equatorial streaming is of a purely Stokesian nature, in contrast to the inertia dominated droplet splash and sheet disintegration [30–33]. Moreover, the interface polarization (charging) is much faster than the interface deformation due to the electrohydrodynamic flow (as seen by comparing the Maxwell-Wagner and electrohydrodynamic time scales: $t_{mw} = \varepsilon_{\rm ex}(S+2)/\sigma_{\rm ex}(R+2) \sim 1$ms, and $t_{ehd} = \mu_{\rm ex}(1+\lambda)/\varepsilon_{\rm ex}E^2 \sim 10$ ms.) Hence, the streaming in our system is controlled by the shear stresses [2, 3], very much like in flow focusing, i.e. tip-streaming induced by co-flowing two fluids [34], and in contrast to the unsteady electrospray [35], where charge relaxation is non-negligible.

The phenomenon is a multistep process involving a downsizing cascade from one macro-drop, to a thin edge-sheet, to concentric fluid rings, to thousands of microdroplets, see Figure 4.

At the onset of streaming, the drop forms a sharp edge at the equator from which a thin-sheet extends. The critical capillary number can be estimated from linear stability analysis [6], which predicts that the cutoff instability wavenumber k^*a depends on the field strength as $k^*a = 0.55\,Ca$ for our system [19]. For the instability to occur the shortest unstable wavelength has to be smaller than the natural cutoff length (the drop perimeter), i.e. $k^*a > 2$, which gives Ca_c of about 3.6 in good agreement with the experimental observations. This suggests the following qualitative picture for the onset of streaming: A perturbation on the interface near the stagnation

equatorial line gets entrained by the converging flow to form a sheet. The surface tension opposes the interface deformation but its effect is weakened by the electric stresses. Indeed, the electric pressure increases significantly as the drop flattens compared to a sphere and becomes more localized near the equator (see [19]). Moreover, the shear electric stresses which drive the convergent flow strengthen as the aspect ratio increases. Both effects - stronger electric pressure and shear stress aid the growth of the instability. In contrast to the EHD cone-jetting, the sheet and subsequently formed structures (rings and drops) are charge-free because the stagnation line is the location of zero induced charge, e.g., for a sphere the induced charge varies as $\cos\theta$.

In a second step, the sheet pinches off at the leading edge and sheds rings with a typical radius r_c about $20\mu m$, see Figure 4. Unlike a cylindrical thread, an infinite planar thin film is capillary stable. However, the applied electric field can destabilize the film [37] because of the opposite sign of the induced charge on the film interfaces. The theory predicts cutoff wavenumber $k^*h \sim 2\zeta^{1/2}$, where h is the film thickness and $\zeta = \varepsilon_{\rm ex}E^2h/\gamma \equiv Ca\,h/a$. The film thickness h can be estimated from volume conservation: the volume in a section of the thin film spanned by a wavelength $\xi = 2\pi/k^*$ after pinch off is transferred into a ring with radius r_c; hence $h\xi = \pi r_c^2$ (per unit edge length). Thus we find $h \sim \left(r_c^4\,Ca/a\right)^{1/3}$. For the $\lambda = 0.07$ drop fluid, $h \sim 10\,\mu$m.

In a final step, the rings break into droplets via the classical capillary instability. The linear stability analysis predicts wavelength $c(\lambda)r_c$, where $c(\lambda)$ ranges from 24.4 to 11 for viscosity ratios $\lambda = 0.001 - 0.1$ [38]. For $\lambda = 0.07$, we measure wavelength $200\mu m$ which is in very good agreement with the theory. The concentric rings break up via an out-of-phase correlation between neighboring rings: due to hydrodynamic interactions an alternation of necking and expanding occurs along the orthogonal direction [39], see Figure 4.c. The capillary instability is also characterized by the formation of satellite droplets during breakup. The ratio of droplet diameter from generation to mother is a function the viscosity ratio [40]. For $\lambda = 0.07$, the daughter-mother size ratios of the two generations visible in our experiments, indicated by the blue arrows on Figure 4.c, is about 0.2 and 0.1, in good agreement with the numerical predictions. One generation of a satellite cylinder is also created as a ring detaches from the edge-sheet, see Figure 4.d.

The final outcome of the streaming is the formation of thousands of microdroplets of quite uniform in size, see Figure 5. The average radius increases with the viscosity ratio as $\lambda^{1/2}$. This power-law dependency seems to originate from the slenderness of the sheet from which the cylinders are formed. According to slender body theory for a thin film of length L and thickness $h \sim r_c$, the balance of viscous shear stresses imposed by the external flow, $\mu_{\rm ex}U/L$, and lubrication pressure in the thin film, $\lambda\mu_{\rm ex}UL/h^2$ yields $h/L \sim \lambda^{1/2}$ [41]. Since the rings break-up via capillary instability, droplet size is set by the cylinder radius and follows the same dependence on viscosity ratio.

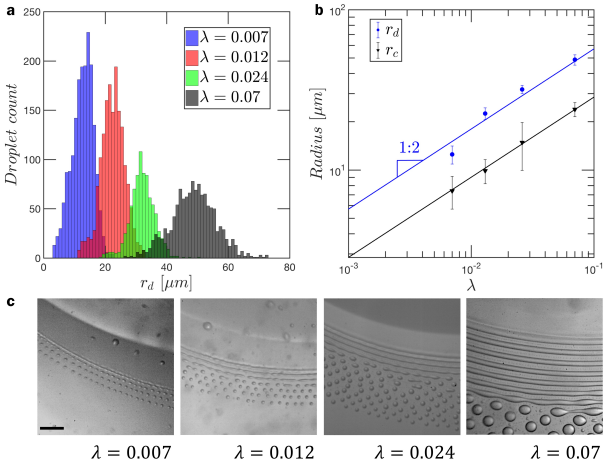

FIG. 5: (Color online) (a) Droplet size distribution at different viscosity ratio λ. Standard deviation varies between $15-30\%$ of the central value. (b) Ring r_c and droplet r_d radii follow $\sim \lambda^{1/2}$ dependence on viscosity ratio. (c) The number of concentric rings decreases with decreasing viscosity ratio; a ring is barely visible at $\lambda = 0.007$ and the droplets seem to originate directly from the edge-sheet. Scale bar $200\mu m$.

Concluding remarks: In this Letter we report that upon application of a uniform DC electric field, a drop flattens, forms a sharp edge with a thin film attached to it (edge-sheet) shedding charge-free fluid rings encircling the drop. The concentric fluid rings subsequently undergo capillary instability and break up into droplets. The droplets form an initially hexagonal pattern in the equatorial plane of the mother drop. The streaming occurs only for low viscosity drops, with viscosity ratio smaller than 0.1 and field strengths corresponding to $Ca \geq 4$.

While the detailed mechanism of the streaming is yet to be quantified, the phenomenon is reasonably explained by the interfacial instability of the stagnation line of a convergent flow [6]. The flow is driven by electric shear stresses on the drop interface and converges at the equator. A perturbation of the compressed interface grows and a fluid sheet is drawn from the equator, which is the stagnation line. The growth of the interface deformation into an edge-sheet structure is aided by he normal electric stresses which overcome the surface tension.

EHD equatorial streaming allows the production of large number of micro-droplets in a relatively short time. The final droplet size can be tuned by changing the viscosity ratio. This study suggests ways of microdroplets

production in bulk environment, "electroemulsification", with potential application in industrial processes.

We hope our experimental observations will inspire further work into this phenomenon. Numerical simulations are needed to explain the effects of viscosity ratio and field strength in the selection of the "streaming" versus the "dimpling" mode of drop destabilization. The nature of the instability suggests that equatorial streaming from a drop can be obtained in absence of electric field, for example, a surfactant-covered drop in axisymmetric compressional flow.

Acknowledgements: This research was supported by the NSF - CBET 1437545 and CMMI-1538703 awards.

* Present address: Engineering Sciences and Applied Mathematics, Northwestern University, Evanston, IL 60208, USA

[1] J. F. de la Mora. *Annu. Rev. Fluid. Mech.*, 39:217–243, 2007.
[2] R. T. Collins, K. Sambath, M. T. Harris, and O. A. Basaran. *PNAS*, 110:4905–4910, 2013.
[3] R. T. Collins, J. J. Jones, M. T. Harris, and O. A. Basaran. *Nature Physics*, 4:149–154, 2008.
[4] E. O. Elele, Y. Shen, D. R. Pettit, and B. Khusid. *Phys. Rev. Lett.*, 114:054501, 2015.
[5] O. A. Basaran, H. Gao, and P. P. Bhat. *Annu. Review Fluid Mech.*, 45:85–113, 2013.
[6] Y.-H. Tseng and A. Prosperetti. *J. Fluid Mech.*, 776:5–36, 2015.
[7] R. Suryo and O. A. Basaran. *Phys. Fluids*, 18:082102, 2006.
[8] E. Castro-Hernandez, F. Campo-Cortes, and J. Manuel Gordillo. *J. Fluid Mech.*, 698:423–445, 2012.
[9] S. L. Anna. *Annu. Rev. Fluid Mech.*, 48:285–309, 2016.
[10] J Eggers. *Phys. Rev. Lett.*, 86:4290–4293, 2001.
[11] G. I. Taylor. *Proc. R. Soc. A*, 291:159–166, 1966.
[12] J. R. Melcher and G. I. Taylor. *Annu. Rev. Fluid Mech.*, 1:111–146, 1969.
[13] E. Lac and G. M. Homsy. *J. Fluid. Mech*, 590:239–264, 2007.
[14] O. Ghazian, K. Adamiak, G. S. P. Castle, and Y. Higashiyama. *Coll. Surf. A*, 441:346–353, 2014.
[15] M. Zabarankin, I. Smagin, O. M. Lavrenteva, and A. Nir. *J. Fluid. Mech.*, 720:169–191, 2013.
[16] S. Torza, R.G. Cox, and S.G. Mason. *Phil. Trans. Royal Soc. A*, 269:295–319, 1971.
[17] A. S. Mohamed, J. M. Lopez-Herrera, M. A. Herrada, L. B. Modesto-Lopez, and A. M. Ganan-Calvo. *Langmuir*, 32:6815–6824, 2016.
[18] P. F. Salipante and P. M. Vlahovska. *Phys. Fluids*, 22:112110, 2010.
[19] See Supplemental Material [URL] for more details about the experimental system and the theoretical models, which includes Refs. [20-23].
[20] H. Nganguia, Y. N. Young, P. M. Vlahovska, J. Blawzdziewcz, J. Zhang, and H. Lin. *Phys. Fluids*, 25:092106, 2013.
[21] H. Nganguia and Y. N. Young. *Phys. Rev. E*, 88:052718, 2013.
[22] P.G.. Drazin. *Introduction to hydrodynamic stability.* Cambridge University Press, 2002.
[23] P. M. Vlahovska. *J. Fluid Mech.*, 670:481–503, 2011.
[24] P. M. Vlahovska. *Phys. Rev. Fluids*, 1:060504, 2016.
[25] E. Yariv and I. Frankel. *J. Fluid Mech.*, 788:R2, 2016.
[26] H. He, P. F. Salipante, and P. M. Vlahovska. *Phys. Fluids*, 25:032106, 2013.
[27] P. F. Salipante and P. M. Vlahovska. *Phys. Rev. E*, 88:043003, 2013.
[28] T. B. Jones. *IEEE Trans. Industry Appl.*, 20:845–849, 1984.
[29] E. Pairam and A. Fernández-Nieves. *Phys. Rev. Lett.*, 102:234501, 2009.
[30] G. I. Taylor. *Proc. R. Soc. Lond. A*, 253:313–321, 1959.
[31] C. Clanet. *Annu. Rev. Fluid Mech*, 39:469–496, 2007.
[32] J. Eggers and E. Villermaux. *Rep. Prog. Phys.*, 71:036601 2008.
[33] L. V. Zhang, P. Brunet, J. Eggers, and R. D. Deegan. *Phys. Fluids*, 22:122105 2010.
[34] A. M. Ganan-Calvo and J. M. Montanero. *Phys. Rev. E*, 79:066305, 2009.
[35] A. M. Ganan-Calvo, J. M. Lopez-Herrera, N. Rebollo-Munoz, and J. M. Montanero. *Scientific reports*, 6:32357, 2016.
[36] J. A. Lanauze, L. M. Walker, and A. S. Khair. *J. Fluid Mech.*, 774:245–266, 2015.
[37] D. H. Michael and M.E. O'Neill. *J. Fluid. Mech.*, 41:571–580, 1970.
[38] S. Tomotika. *Proc. R. Soc. London. A*, 150:322–337, 1935.
[39] Z. Zhang, G. C. Hilton, R. Yang, and Y. Ding. *Soft Matter*, 11:7264–7269, 2015.
[40] M. Tjahjadi, H.A. Stone, and J.M. Ottino. *J. Fluid Mech.*, 243:297–317, 1992.
[41] H. A. Stone. *Annu. Rev. Fluid Mech.*, 26:65–99, 1994.